
This is an electronic reprint of the original article.
This reprint may differ from the original in pagination and typographic detail.

Ma, Xiaofeng; Sarkka, Simo

Spacing Vector and Varying Distance Constrained Positioning Using Dual Feet-Mounted IMUs

Published in:
IEEE Transactions on Instrumentation and Measurement

DOI:
[10.1109/TIM.2024.3472776](https://doi.org/10.1109/TIM.2024.3472776)

Published: 01/01/2024

Document Version
Publisher's PDF, also known as Version of record

Published under the following license:
CC BY

Please cite the original version:
Ma, X., & Sarkka, S. (2024). Spacing Vector and Varying Distance Constrained Positioning Using Dual Feet-Mounted IMUs. *IEEE Transactions on Instrumentation and Measurement*, 73.
<https://doi.org/10.1109/TIM.2024.3472776>

This material is protected by copyright and other intellectual property rights, and duplication or sale of all or part of any of the repository collections is not permitted, except that material may be duplicated by you for your research use or educational purposes in electronic or print form. You must obtain permission for any other use. Electronic or print copies may not be offered, whether for sale or otherwise to anyone who is not an authorised user.

Spacing Vector and Varying Distance Constrained Positioning Using Dual Feet-Mounted IMUs

Xiaofeng Ma^{ID}, *Graduate Student Member, IEEE*, and Simo Särkkä^{ID}, *Senior Member, IEEE*

Abstract—The zero velocity update (ZUPT) offers an effective correction method for sensor drift in indoor positioning systems using foot-mounted inertial measurement units (IMUs). However, the heading drift is still a problem in positioning systems using IMUs. This article develops methods for positioning using two foot-mounted IMUs to solve this problem. The proposed method is based on the use of a time-varying distance constraint (VDC) and a spacing-vector constraint. Our methods are experimentally compared against other distance-constraint-based methods using a dataset that we collected for this purpose. The results show that our method has better control of the separation between the trajectories of the feet.

Index Terms—Distance constraint, dual inertial measurement units (IMUs), foot mounted, indoor positioning, spacing-vector constraint.

I. INTRODUCTION

INERTIAL measurement units (IMUs) are highly effective for positioning in environments where infrastructure-based positioning systems (e.g., GPS [1] or Wi-Fi [2]) are not available. In particular, MEMS-based IMUs are popular in personal positioning systems because they are economical, self-contained, and compact enough to be wearable or integrated into a smartphone [3]. IMU-based pedestrian dead reckoning (PDR) systems can be classified into step-and-heading systems (SHSs) and strap-down inertial navigation systems (SINSs) [3], [4]. The former is specific to pedestrians and computes a 2-D planar trajectory by accumulating the distance by counting the steps and tracking the heading with a gyroscope or magnetometer. The latter obtains 3-D displacement by double integration of the acceleration expressed in the navigation coordinate system. However, the accumulation of sensor errors makes both types of PDRs unreliable for longer periods of time [5].

Using a foot-mounted IMU is an effective solution to the error accumulation problem. The periodic contacts of the foot with the ground can be used as pseudo-measurements for drift corrections. This technology is known as zero velocity updates (ZUPTs) [5]. Hou and Bergmann [3] reviewed hundreds of papers related to pure IMU-based PDRs and found that studies

using foot-mounted IMUs generally have a higher accuracy. However, the heading-related states are not observable from the zero velocity pseudo-measurements, which leads to a heading drift in the calculated trajectory. To reduce this drift, recent research has focused on using additional devices such as distance sensors, magnetometers, and fusing multiple IMUs with physical constraints. We discuss these in the following.

As it is difficult to observe the heading-related states by relying only on the IMU itself, additional sensors can be used to provide reference measurements. For example, Xia et al. [6] use an ultrasonic sensor to detect changes in foot-to-wall distance to determine if there is a heading drift in the current calculated trajectory. However, adding more sensors like this may result in a bulky and cumbersome device.

Magnetometers are also often used to obtain heading information as they can be integrated into an IMU. However, indoor environments may contain ferromagnetic materials that can interfere with the Earth's magnetic field [2]. One way to aid IMU-based positioning is to treat the disturbed magnetic field as a map of fingerprints [2]. To avoid the large effort of collecting a magnetic fingerprint map, Gaussian process regression can be used to estimate the magnetic field [7], [8]. Viset et al. [9] developed a method for simultaneous localization and mapping of magnetic field using an extended Kalman filter (EKF). Nevertheless, Gaussian process regression methods for magnetic field-based positioning have difficulties in providing good predictions for unexplored areas.

The use of multiple IMUs on a single leg is another research area. In [10], the joint equality constraint between the lateral side of the shoe and the calf is analyzed and used as an observation for EKF. Li et al. placed IMUs on the upper sides of the ankle and the toe in paper [11] and added one more IMU on the heel in paper [12]. The authors analyzed the geometry of the placements during the swing and stance phases. The velocity and position relationships between the IMUs are then used as observations for measurement updates. Wang et al. [13] placed IMUs on the calf and the ipsilateral instep, and derived an angle constraint, a degree-of-freedom constraint, and a relative-position constraint existing between the two IMUs due to the structure of the human body. These constraints were then used for state estimation of the two IMUs. However, the observability of drift due to heading in the above constraints or measurements is yet unclear.

Another kind of approach, which we also study here, is to place sensors on both feet. The drift can then be diminished by limiting the distance between the feet [14], [15], [16], [17],

Received 2 June 2024; revised 13 August 2024; accepted 2 September 2024. Date of publication 3 October 2024; date of current version 18 October 2024. The work of Xiaofeng Ma was supported in part by the Program of China Scholarships Council (CSC) under Grant 202106020074 and in part by the Research Council of Finland. The Associate Editor coordinating the review process was Dr. Gabriele Patrizi. (*Corresponding author: Xiaofeng Ma.*)

The authors are with the Department of Electrical Engineering and Automation, Aalto University, 02150 Espoo, Finland (e-mail: xiaofeng.ma@aalto.fi; simo.sarkka@aalto.fi).

Digital Object Identifier 10.1109/TIM.2024.3472776

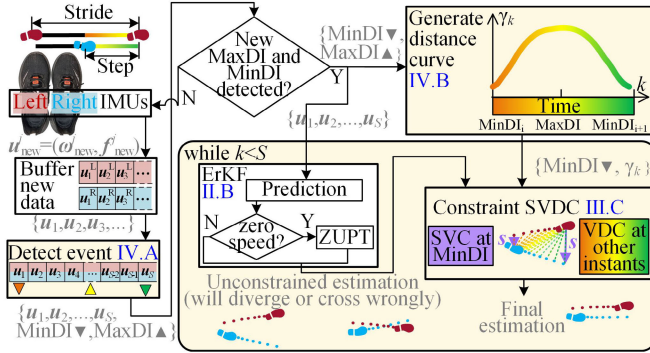


Fig. 1. Illustration of the concept of this article. The trajectories of two feet calculated in one stride by independent ZUPT-aided ErKF diverge due to drifts, shown as unconstrained estimation where the footprints represent stance phases. We develop new methods (in light yellow-filled boxes) to constrain them, where VDC is a distance constraint applied to each instant shown as a color gradient and SVC is a vector constraint applied to MinDIs shown as purple arrows. Using these physical constraints, the drift in the final trajectory estimate is reduced.

[18], [19], [20], [21], [22], [23]. In paper [14], the problem is formulated as an optimization problem with an inequality constraint. Prateek et al. [15] give a closed-form solution for constraining the position of the swinging foot. Bolotin et al. [16] regard the maximum distance as a pseudo-observation for an EKF. Shi et al. [17] argue that an ellipsoidal boundary is more suitable than a spherical boundary because the height difference between the two feet in walking is more constrained than the horizontal distance. Wang et al. [18] calculate the distance between the feet using the estimated feet position at the start of each stride (the two are both in stance phase) as the maximum bound for the current stride.

In practice, the maximum distance constraint (MaxDC) is rather loose and the constraint on drift is lagging. The actual distance between the feet varies from a maximum to a minimum and then increases again. To get a more real-time distance between feet, Jao et al. [19] put two cameras at heels with a chessboard pattern. Then, a relative position measurement between the two is given when the cameras can see each other. Zhu et al. [20] and Qi et al. [21] take the real-time range measurement from two ultrasonic sensors mounted on each foot as observations for EKF. Chen et al. [22] showed that ultra-wideband (UWB) sensors can provide better measurements in nonline-of-sight (NLoS) scenarios compared to ultrasonic sensors. However, ground and orientation effects still require extra processing due to the UWB being mounted on feet. Moreover, these additional sensors and the corresponding data processing make the whole system more complicated.

In paper [23], the minimum foot-to-foot distance, which occurs when the moving foot passes by the standing foot, is taken as a pseudo-measurement for EKF. The minimum distance constraint (MinDC) bounds the drift in a more timely manner than the MaxDC. In paper [24], we proposed an inequality distance constraint that considers both maximum and minimum bounds and even intermediate instant bounds, using an assumed time-varying distance curve. In the same paper, we also proposed a spacing vector constraint (SVC) that is enabled when the feet are side-by-side. It takes into account the spatial physical limitations of the left and right feet. In this

article, we replace the inequality constraints with equality constraints using an experimentally determined distance curve.

Positioning using an array of IMUs is also possible and has turned out to have a good practical performance [25], [26]. It allows using statistical means to obtain better positioning results from the IMU array by canceling out the noise. However, the cost, number of IMUs, and size of the module affect the accuracy and relative performance of the IMU array-based methods.

This article is an extension of our work [24]. Here, we focus on the time-varying distance equality constraint without additional sensors. The flowchart of the system is illustrated in Fig. 1. The contributions are summarized as follows.

- 1) We propose a dual-feet positioning method with time-varying distance equality constraint requiring only IMU sensors, which we call spacing vector and VDC (SVDC), that can provide constraints for the feet at each instant.
- 2) We perform a series of experiments to determine the regularity patterns for the feet spacing to aid the construction of an experimental distance curve model for the feet.
- 3) Based on the experimental data, we propose a model for the distance curve between two insteps and its adaptive deformation. It provides time-varying distance pseudo-measurements without additional sensors.
- 4) We experimentally compare our method with other methods on different paths and different subjects. The effect of different settings of the proposed distance curve on the results is also shown. The dataset will be made publicly available after this article is accepted.

The structure of this article is the following. In Section II, we explain some of the terms related to walking movements that will be used throughout the text and describe the implementation of the ZUPT-only method which we use as a baseline. The proposed methods are explained in Sections III and IV. The collected datasets are explained and the methods are compared in Section V. Finally, we conclude our work in Section VI.

II. ZUPT-AIDED PEDESTRIAN POSITIONING

In this section, we define some terms related to walking and also define the basic dual-foot model that uses only ZUPT method.

A. Gait Cycle

Human walking is a periodic movement known as the gait cycle which can be divided into gait phases by gait events [27]. Fig. 2 shows a healthy gait pattern represented by frontal angular velocity, and the corresponding gait phases and events based on papers [27], [28], [29]. For ease of statement, the often-mentioned terms in this article are explained as follows.

- 1) *Step*: The distance between two feet while standing.
- 2) *Stride*: The distance between two consecutive footfalls of one foot, which generally equals two steps (see Fig. 1).
- 3) *Zero Velocity Interval (ZVI)*: The foot is almost static and the ZUPT technology is implemented in this period.

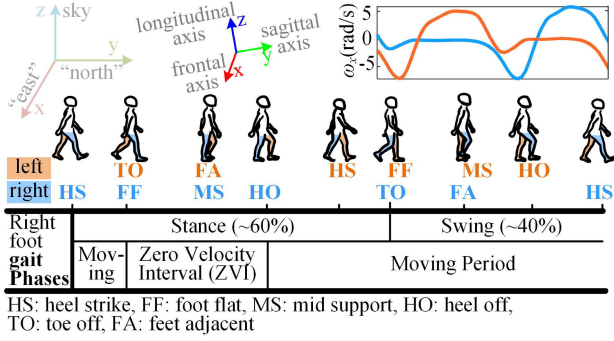


Fig. 2. Illustration of a gait cycle, important terms, and the corresponding foot angular velocity of the frontal axis.

4) *Minimum Distance Instant (MinDI)* or *Maximum Distance Instant (MaxDI)*: The instants when the feet are closest to each other or farthest from each while walking. The detection of gait phases and events can help the positioning method to find the instants at which constraints or measurements are implemented. The specific detection methods will be described in Section IV-A.

B. Positioning With ZUPT

Next, we describe the model often used in foot-mounted IMUs, the error-state Kalman filter (ErKF) [30], which we also use in the dual-foot case. Taking position, velocity, quaternion, and accelerometer biases as the states of j th system ($j \in \{R, L\}$ means right or left), the navigation model is [31]

$$\begin{bmatrix} \mathbf{p}_k^j \\ \mathbf{v}_k^j \\ \mathbf{q}_k^j \\ \mathbf{b}_{a,k}^j \end{bmatrix} = \begin{bmatrix} \mathbf{p}_{k-1}^j + \mathbf{v}_{k-1}^j T_s \\ \mathbf{v}_{k-1}^j + T_s (\mathbf{C}_b^n (\mathbf{f}_{k-1}^j - \mathbf{b}_{a,k-1}^j) + \mathbf{g}^n - \mathbf{w}_{a,k-1}^j) \\ \mathbf{q}_{k-1}^j \otimes \exp\left(\frac{T_s}{2} (\boldsymbol{\omega}_{k-1}^j - \mathbf{w}_{g,k-1}^j)\right) \\ \mathbf{b}_{a,k-1}^j + \mathbf{w}_{ba,k-1}^j \end{bmatrix} \quad (1)$$

$$\mathbf{x}_k^j = \mathbf{f}(\mathbf{x}_{k-1}^j, \mathbf{u}_{k-1}^j, \mathbf{w}_{k-1}^j)$$

where T_s is the sampling time, \mathbf{C}_b^n is the direction cosine matrix from the body frame to the navigation frame, $\mathbf{g}^n = [0 \ 0 \ -g]^\top$ is the gravity, $\mathbf{u}_k^j = [\mathbf{f}_k^{j\top} \ \boldsymbol{\omega}_k^{j\top}]^\top$ is the output of IMU including the specific force and the angular velocity, and $\mathbf{b}_{a,k}^j$ is the accelerometer bias vector. Furthermore, $\mathbf{w}_k^j = [\mathbf{w}_{a,k}^{j\top} \ \mathbf{w}_{g,k}^{j\top} \ \mathbf{w}_{ba,k}^{j\top}]^\top$ are Gaussian noises with zero means and covariances $\mathbf{Q}^j = \text{diag}(\sigma_a^2 \mathbf{I}_3, \sigma_g^2 \mathbf{I}_3, \sigma_{ba}^2 \mathbf{I}_3)$ for the accelerometers, gyroscopes, and accelerometer biases, respectively. Above, \otimes denotes the quaternion product and $\exp(\cdot)$ is the quaternion exponential.

The ZUPT model [5] is

$$\mathbf{y}_k^j = \mathbf{v}_k^j + \mathbf{r}_k^j \quad (2)$$

where the pseudo-measurement $\mathbf{y}_k^j \triangleq \mathbf{0}$ and \mathbf{r}_k^j is a zero-mean Gaussian measurement noise with covariance \mathbf{R}^j which can be set to a suitable small value, for example, $\mathbf{R}^j = 0.0001 \mathbf{I}_3$.

Note that we have not included the gyroscope biases in the model. This is because estimating IMU biases simultaneously does not always enhance the performance [32]. In our experience, including gyroscope biases may even make the performance worse as they are not observable from the zero-velocity measurements [5], [33]. Therefore, we only include

biases of the accelerometer into the state in addition to the navigation states.

In a dual feet system, the navigation states are $\mathbf{x}_k = [(\mathbf{x}_k^R)^\top (\mathbf{x}_k^L)^\top]^\top$, where \mathbf{x}_k^R and \mathbf{x}_k^L are the states, similar to (1), for the left and right feet, respectively. The ErKF [30] estimates error-state $\delta \mathbf{x}_k$ (error in \mathbf{x}_k) by a Kalman filter and uses it to update the nominal state. The procedure is as follows [30], [34].

- 1) Perform a dynamic update of nominal state by

$$\hat{\mathbf{x}}_k^- = \begin{cases} \mathbf{f}(\hat{\mathbf{x}}_{k-1}^+, \mathbf{u}_{k-1}^R) \\ \mathbf{f}(\hat{\mathbf{x}}_{k-1}^+, \mathbf{u}_{k-1}^L) \end{cases} \quad (3)$$

where $-$ denotes a priori or predicted, $+$ denotes a posteriori or corrected, and $\hat{\cdot}$ indicates an estimate.

- 2) Predict the error state and covariance

$$\delta \hat{\mathbf{x}}_k^- = \mathbf{F}_{k-1} \delta \hat{\mathbf{x}}_{k-1}^+ = 0 \quad (4a)$$

$$\mathbf{P}_k^- = \mathbf{F}_{k-1} \mathbf{P}_{k-1}^+ \mathbf{F}_{k-1}^\top + \mathbf{L}_{k-1} \mathbf{Q}_{k-1} \mathbf{L}_{k-1} \quad (4b)$$

where (4a) holds because $\delta \hat{\mathbf{x}}_{k-1}^+$ was reset to zero in the last loop [also see (6b)], \mathbf{P}_k is the state covariance, $\mathbf{Q}_k = \text{blockdiag}(\mathbf{Q}^R, \mathbf{Q}^L)$, $\mathbf{L}_k = \text{blockdiag}(\mathbf{L}_k^R, \mathbf{L}_k^L)$, and $\mathbf{F}_k = \text{blockdiag}(\mathbf{F}_k^R, \mathbf{F}_k^L)$. For the details of \mathbf{F}_k^j and \mathbf{L}_k^j , see [14], [15], [31], and [35].

- 3) Perform measurement update on the error state (below, ZVD refers to zero velocity detection)

$$\mathbf{H}_k = \begin{cases} \begin{bmatrix} \mathbf{H}_0 & \mathbf{0}_{3 \times 12} \end{bmatrix}, & \text{only right ZVD is true} \\ \begin{bmatrix} .5pc \end{bmatrix} \begin{bmatrix} \mathbf{0}_{3 \times 12} & \mathbf{H}_0 \end{bmatrix}, & \text{only left ZVD is true} \\ \begin{bmatrix} .5pc \end{bmatrix} \begin{bmatrix} \mathbf{H}_0 & \mathbf{0}_{3 \times 12} \\ \mathbf{0}_{3 \times 12} & \mathbf{H}_0 \end{bmatrix}, & \text{both ZVDs are true} \end{cases} \quad (5a)$$

$$\mathbf{K}_k = \mathbf{P}_k^- \mathbf{H}_k^\top (\mathbf{R}_k + \mathbf{H}_k \mathbf{P}_k^- \mathbf{H}_k^\top)^{-1} \quad (5b)$$

$$\delta \hat{\mathbf{x}}_k^+ = -\mathbf{K}_k \mathbf{H}_k \delta \hat{\mathbf{x}}_k^- \quad (5c)$$

$$\mathbf{P}_k^+ = (\mathbf{I} - \mathbf{K}_k \mathbf{H}_k) \mathbf{P}_k^- \quad (5d)$$

where $\mathbf{H}_0 = [\mathbf{0}_3 \ \mathbf{I}_3 \ \mathbf{0}_{3 \times 6}]$ and \mathbf{R}_k is the block diagonal matrix of \mathbf{R}^R and \mathbf{R}^L .

- 4) Update the nominal state and reset the error state

$$\hat{\mathbf{x}}_k^+ = \hat{\mathbf{x}}_k^- + \delta \hat{\mathbf{x}}_k^+ \quad (6a)$$

$$\delta \hat{\mathbf{x}}_k^+ = 0. \quad (6b)$$

III. DISTANCE CONSTRAINTS FOR TWO FEET

When using the method above, there are still increasing errors in the position and yaw estimates over time when using ZUPT, because the position, the yaw angle, and the vertical gyroscope bias are unobservable from zero velocity measurements [5], and because in the model, the motions of the two feet are independent. In this section, we introduce and propose methods for the dual feet-mounted IMU case that model the dependence between the feet. First, two range-constrained methods, MaxDC [36] and MinDC [37] are reviewed. Then, we develop a new SVDC method, which is a combination and improvement of our separate VDC and SVC proposed in [24].

A. Constant MaxDC

The underlying idea of MaxDC is that the distance between two feet should be less than a constant value γ . Here, we introduce one implementation proposed in work [36], which will also be compared with in the experimental results in Section V.

The MaxDC is formulated as an optimization problem with a nonlinear inequality constraint

$$\tilde{\mathbf{p}}_k = \arg \min_{\mathbf{p} \in \mathbb{R}^6} (\|\hat{\mathbf{p}}_k^+ - \mathbf{p}\|_2^2), \text{ s.t. } \|\mathbf{p}_k^R - \mathbf{p}_k^L\|_2^2 \leq \gamma_{\max}^2 \quad (7)$$

where $\tilde{\mathbf{p}}_k = [\tilde{\mathbf{p}}_k^{R\top} \ \tilde{\mathbf{p}}_k^{L\top}]^\top$ contains the position estimates of the right and left feet and γ_{\max} is the preset upper bound of the distance between two feet.

The solution to the problem obtained using the Lagrange multiplier method is [36] when $\hat{d}_k^2 > \gamma_{\max}^2$

$$\tilde{\mathbf{p}}_k^R = \frac{1}{2}(\hat{\mathbf{p}}_k^R + \hat{\mathbf{p}}_k^L) + \frac{\gamma_{\max}}{2\hat{d}_k}(\hat{\mathbf{p}}_k^{R+} - \hat{\mathbf{p}}_k^{L+}) \quad (8a)$$

$$\tilde{\mathbf{p}}_k^L = \frac{1}{2}(\hat{\mathbf{p}}_k^{R+} + \hat{\mathbf{p}}_k^{L+}) - \frac{\gamma_{\max}}{2\hat{d}_k}(\hat{\mathbf{p}}_k^R - \hat{\mathbf{p}}_k^L) \quad (8b)$$

where $\hat{d}_k = \|\hat{\mathbf{p}}_k^{R+} - \hat{\mathbf{p}}_k^{L+}\|_2$ is the distance between the two feet computed using the Kalman a posteriori estimate.

Finally, when $\hat{d}_k > \gamma_{\max}$, the coordinates calculated from (8) are used as pseudo-measurements with noise covariance \mathbf{R}_{pos} for a further measurement update after ZUPT.

B. Minimum Distance Constraint

Liu et al. [37] show that the maximum distance between the feet is not stable. It varies with speed or even with different strides at the same speed. It can also lead to untimely constraints if the bound γ is set too loosely. The fluctuation of the minimum distance is proved to be smaller in various walking speeds and pattern scenarios [37]. Hence, Liu et al. [37] proposed to use a MinDC. The minimum distance was experimentally determined to occur at 60% of the ZVI in their work. Note that the conclusion in this article is drawn in a configuration that the IMUs are placed at heels and the ZVIs are detected using the SHOE method.

The constraint is formulated as an optimization problem

$$\tilde{\mathbf{x}}_k = \arg \min_{\mathbf{x}_k \in \mathbb{R}^{18}} (\|\hat{\mathbf{x}}_k^+ - \mathbf{x}_k\|_{\mathbf{P}_k^{-1}}^2), \text{ s.t. } \|\mathbf{p}_k^R - \mathbf{p}_k^L\|_2^2 = \gamma_{\min}^2 \quad (9)$$

and the solution of the problem by projection approach is

$$\tilde{\mathbf{x}}_k = \hat{\mathbf{x}}_k^+ - \mathbf{P}_k \mathbf{A}_k^\top (\mathbf{A}_k \mathbf{P}_k \mathbf{A}_k^\top)^{-1} (\mathbf{A}_k \hat{\mathbf{x}}_k^+ - b). \quad (10)$$

Then, the navigation states are updated iteratively at $k = \text{MinDI}$ starting from the a posteriori estimate of ErKF-ZUPT at MinDI (for more details, see [37]).

C. Proposed SVDC

We proposed two constraints in paper [24]. The first is VDC, which follows the idea of MaxDC but replaces the fixed maximum bound γ_{\max} with a simulated time-varying bound γ_k . The second is SVC, which can correct the wrong crossing of the left and right feet as shown in Fig. 1. These two methods

are used as separate methods in [24]. Here, we combine and improve them which leads to the proposed SVDC method.

The constraints in our method are incorporated by including a nonlinear constraint to a Kalman filter. Suppose that we have a nonlinear constraint on \mathbf{x}_k

$$g(\mathbf{x}_k) = c \quad (11)$$

where c is a constant. Linearize (11) around $\hat{\mathbf{x}}_k^+$

$$g(\mathbf{x}_k) \approx g(\hat{\mathbf{x}}_k^+) + \mathbf{G}_k(\mathbf{x}_k - \hat{\mathbf{x}}_k^+) \quad (12)$$

the corresponding linearized constraint on the error states $\delta\mathbf{x}_k = \mathbf{x}_k - \hat{\mathbf{x}}_k^+$ can be derived as

$$\mathbf{G}_k \delta\mathbf{x}_k = c_k \quad (13)$$

where $\mathbf{G}_k = (\partial g(\mathbf{x})/\partial \mathbf{x})|_{\mathbf{x}=\hat{\mathbf{x}}_k^+}$ and $c_k = c - g(\hat{\mathbf{x}}_k^+)$.

The constraints can be incorporated into the Kalman filter, for example, by a projection method, augmented perfect measurements, or as a soft constraint [38]. The projection and perfect measurements approach are suitable for strict mathematical constraints and the soft approach is suitable for constraints that are heuristic rather than rigorous [38], [39].

Here, the constraints are implemented as soft constraints considering they are heuristic. The problem is then to minimize the following cost function for $\delta\tilde{\mathbf{x}}_k$:

$$J = \|\delta\tilde{\mathbf{x}}_k - \delta\hat{\mathbf{x}}_k^+\|_{\mathbf{W}_k}^2 + \|c_k - \mathbf{G}\delta\tilde{\mathbf{x}}_k\|_{\mathbf{R}_c^{-1}}^2 \quad (14a)$$

$$= \|\delta\tilde{\mathbf{x}}_k\|_{\mathbf{W}_k}^2 + \|c_k - \mathbf{G}\delta\tilde{\mathbf{x}}_k\|_{\mathbf{R}_c^{-1}}^2 \quad (14b)$$

where \mathbf{R}_c is the noise covariance of the constraint and \mathbf{W}_k is a symmetric positive definite weighting matrix [38]. The setting of \mathbf{W}_k will be discussed in Section III-D. Note the constraint is implemented after (6a), $\delta\hat{\mathbf{x}}_k^+$ is therefore equal to $\mathbf{0}$. By $(\partial J/\partial \delta\tilde{\mathbf{x}}_k) = 0$, we get

$$\tilde{\mathbf{P}}_k = \mathbf{P}_k^+ - \mathbf{P}_k^+ \mathbf{G}_k^\top (\mathbf{G}_k \mathbf{W}_k^{-1} \mathbf{G}_k^\top + \mathbf{R}_c)^{-1} \mathbf{G}_k \quad (15a)$$

$$\delta\tilde{\mathbf{x}}_k = \mathbf{W}_k^{-1} \mathbf{G}_k^\top (\mathbf{G}_k \mathbf{W}_k^{-1} \mathbf{G}_k^\top + \mathbf{R}_c)^{-1} c_k. \quad (15b)$$

Finally, the state covariance will be updated according to (15a), and the error state will be updated according to (15b), after which we proceed similar to (6).

The SVDC contains two parts.

1) *Spacing Vector Constraint*: This constraint is active at the MinDI. Due to physical constraints, the trajectories of the feet should not cross when a person walks. Fig. 1 illustrates wrongly inverted trajectories of the feet in the unconstrained estimation. Although the distance constraint method can limit the positions of the two IMUs to a reasonable range, it does not ensure this physical requirement is met. The spacing vector, illustrated by the purple vector \mathbf{s} in Fig. 1 which is the horizontal vector between two feet when the feet are side by side (that is at MinDI), is designed to solve this problem.

Note that here we define the right-front-up coordinate system as the reference system, and the y-axis is pointing toward the ‘‘north,’’ as shown in Fig. 2. Assume that two IMUs are spaced γ_{\min} apart when they are side by side, then we have

$$\begin{bmatrix} p_{x,k}^R \\ p_{y,k}^R \end{bmatrix} - \begin{bmatrix} p_{x,k}^L \\ p_{y,k}^L \end{bmatrix} = \mathbf{C}(\psi_k) \begin{bmatrix} \gamma_{\min} \\ 0 \end{bmatrix} \quad (16)$$

where $p_{x,k}^R$ is the x -coordinate of the right (R) foot, the superscript L indicates the left foot, and similarly for the subscript y . Above, $\mathbf{C}(\psi_k) = \begin{bmatrix} \cos \psi_k & -\sin \psi_k \\ \sin \psi_k & \cos \psi_k \end{bmatrix}$, where ψ_k is the heading of the person. Here, we take the weighted circular average of the two headings of the two IMUs as ψ_k

$$\psi_k = \arctan \frac{\beta^R \sin \psi_k^R + \beta^L \sin \psi_k^L}{\beta^R \cos \psi_k^R + \beta^L \cos \psi_k^L} \quad (17)$$

where ψ_k^j is the heading estimate at k of the j th foot, and β^j is a priori weight of the heading which can be set to 1 if there is no knowledge about them. Substituting (17) into (16)

$$\begin{bmatrix} p_{x,k}^R \\ p_{y,k}^R \end{bmatrix} - \begin{bmatrix} p_{x,k}^L \\ p_{y,k}^L \end{bmatrix} = \gamma_{\min} z^{-\frac{1}{2}} \begin{bmatrix} \beta^R \cos \psi_k^R + \beta^L \cos \psi_k^L \\ \beta^R \sin \psi_k^R + \beta^L \sin \psi_k^L \end{bmatrix} \quad (18a)$$

$$z = (\beta^R)^2 + (\beta^L)^2 + 2\beta^R \beta^L \cos(\psi_k^R - \psi_k^L). \quad (18b)$$

The above equation will be linear with respect to positions if $\psi_{R,k}$ and $\psi_{L,k}$ are set to some heuristic values such as the mean of the heading in a window. In this case, $\mathbf{G}_k = [\mathbf{I}_2 \mathbf{0}_{2 \times 10} \ -\mathbf{I}_2 \mathbf{0}_{2 \times 10}]$ and \mathbf{c}_k is the difference between the right-hand side minus the left-hand side of (18a). It will be nonlinear with respect to positions and headings if $\psi_{R,k}$ and $\psi_{L,k}$ are assumed to be unknown. Then, the constraint needs to be linearized to have the form of (13).

2) *Varying Distance Constraint*: This constraint is active at each instant k except for MinDI. As we explained in Section I, a constant distance constraint may not suffice for compensating the drifting of the two feet. Therefore, we develop a varying distance model that allows for changing the distance constraint in time. Below, we use the notation γ_k for the time-varying bound. The varying distance γ_k could be regarded as a simulated output of the ultrasound module in paper [20] and [21] of each step.

The time-varying constraint is of the form

$$\|\mathbf{p}_{1:2,k}^R - \mathbf{p}_{1:2,k}^L\|_2^2 = \gamma_k^2 \quad (19)$$

where γ_k is the simulated reference distance which will be described in Section IV. Equation (19) needs to be linearized relative to the error state to have the form of (13), which leads to $\mathbf{c}_k = \gamma_k^2 - \|\hat{\mathbf{p}}_{1:2,k}^{R+} - \hat{\mathbf{p}}_{1:2,k}^{L+}\|_2^2$ and $\mathbf{G}_k = [2(\hat{\mathbf{p}}_{1:2,k}^{R+T} - \hat{\mathbf{p}}_{1:2,k}^{L+T}) \mathbf{0}_{1 \times 10} \ -2(\hat{\mathbf{p}}_{1:2,k}^{R+T} - \hat{\mathbf{p}}_{1:2,k}^{L+T}) \mathbf{0}_{1 \times 10}]$.

D. Case Study: Weighting the Feet

The distance constraints can ensure that the two feet are always moving approximately to the same direction. Especially, a distance constraint will correct the trajectories to the truth when the drifts of the two happen to be contralateral, as can be seen from examples in [18], [36], and [40]. However, this direction might not always be correct since the drifts might be ipsilateral, for example, when both the trajectories drift to left. In this case, one of the constrained trajectories may be closer to the truth, but the other may be further away.

It is claimed in [32] that the heading drifts of the two feet are statistically symmetrical, with the majority of left

foot trajectories drifting toward the left and those of the right foot drifting to the right side. The validity of this claim still needs to be further evidenced considering more factors, such as swapping the two IMUs, tests over longer distances (thousands of meters), and more tests (hundreds). Besides, bias instability and random walking of gyroscopes may also lead to different performances between measurements on different time scales.

Our aim is to correct the trajectories closer to the truth even if the drifts are ipsilateral. Intuitively, we hope that the constraint will yield larger corrections to the estimates with higher uncertainty and smaller corrections to the estimates with higher confidence. From (15b), we know that the diagonal elements in \mathbf{W}_k with higher values result in smaller corrections. However, the right and left feet usually have approximately the same confidence in the usual setting of \mathbf{W}_k (e.g., $\mathbf{W}_k = \mathbf{P}_k^-$). Often, we set the same noise parameters for both feet, such as initial state covariance, process noise, or measurement noise. As a result, the amount of correction is roughly the same for both feet, especially at the beginning. Eventually, the two trajectories may only be constrained to the approximate average direction (midway).

Adding different confidence or uncertainty on different feet may help to correct both trajectories to the truth. The problem then is to decide on a logic for formulating an adaptive confidence or uncertainty. For example, increasing process variance \mathbf{Q} in the Kalman filter is conceptually the same as increasing state covariance \mathbf{P} and gain \mathbf{K} [34]. However, the drift regularity of trajectories in reality is atypical and also relates to a person's walking pattern. It is hard to judge which trajectory is relatively better without any absolute reference, such as absolute position or direction. Although determining the relative trajectory confidence is an open question, we show in Section V-D that our method exhibits superior performance to other methods assuming that the said confidence is known.

IV. DISTANCE CURVE CONSTRUCTION

In this section, we describe the construction of the pseudo distance curve used for the method in Section III-C2.

A. Gait Event Detection

To model the varying distance γ_k , we analyzed experimental data that we collected with OptiTrack¹ system. In this section, we will describe the observations from the real data, and based on these, we decide the methods for detecting gait events.

The distances and ZVIs between the feet depend on the marker/sensor placement. Fig. 3(b) shows measured distance curves between two feet for three different marker placements on the feet labeled in Fig. 3(a). The distance between two insteps, between two toes, and between two heels are shown by blue, orange, and yellow solid lines, respectively. The dashed lines are the corresponding ZVIs of the three marker placements constructed using OptiTrack data, where the nonzero values (different amplitudes for clarity) indicate the zero-velocity state of the corresponding placement of one foot. We can see that the MinDIs for the three placements

¹<https://optitrack.com/>

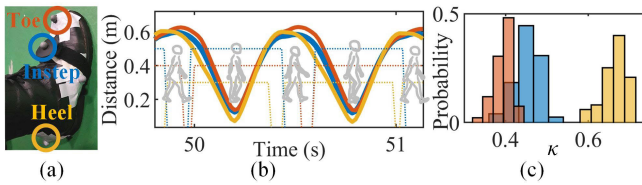


Fig. 3. (b) True distance curves between (a) two insteps, toes, and heels, respectively. The dashed lines are the corresponding ZVIs, where a nonzero value indicates that one of the feet is static. (c) Histogram of the ratio of MinDI to ZVI ($\kappa = (t_{\text{MinDI}} - t_{\text{start of ZVI}}) / (t_{\text{end of ZVI}} - t_{\text{start of ZVI}})$) [37] varies among the three placements. The above are reconstructed from OptiTrack.

differ just a little, but there are noticeable shifts in the MaxDIs. In addition, the start and end of the ZVIs are also different for the three placements.

The MinDI is the instant when the feet are closest to each other, which is hard to detect. Liu et al. [37] found the MinDI is at around 60% of the ZVI, for IMUs installed on heels. However, it is evident from the above that this ratio may vary from placement to placement, as ZVI varies by placement. Fig. 3(c) shows the histogram of the ratio in the three placements computed from OptiTrack data. It can be seen that the ratio is around 45% for the instep and 40% for the toe. For more accurate numbers, more samples should be collected, however, the current evidence is sufficient to show that this ratio varies across different placements. Therefore, the concluded ratio in work [37] is not directly applicable to our IMU placement (on the insteps).

The popular ZVI detector, SHOE, proposed by Skog et al. [41], is used in this article. SHOE detector works well, but sometimes gives incorrect classifications. This can result in the ZVIs being broken by some incorrectly short false MPs. Although these misdetections can be corrected using a set of rules [42], for MinDI detection, we used an alternative method.

To find a suitable method for detecting the MinDIs and MaxDIs, we investigated several variables that were more reflective of the feet's status during forward walking as shown in Fig. 4. From Fig. 4(a), it can be seen that the horizontal velocity of the swinging foot will reach its maximum at the MinDI. The MaxDI occurs approximately at the moment when the speeds of both feet are equal but not zero. From Fig. 4(b), we can see that MaxDI and MinDI do not occur at extremes, over zeros, or intersections of pitch angle, so it is not indicative of MaxDI and MinDI. Similarly, the norm of the specific force is not suitable. From Fig. 4(d), we can see that MinDI can be detected from the maximum peaks of the frontal angular velocity. MaxDIs can be detected by the lowest valleys of the frontal angular velocity. Since velocity requires more calculations compared to the raw sensor data, we use the angular velocity as an indicator of both MinDI and MaxDI.

Furthermore, we compared the gaps between MinDIs and MaxDIs detected from OptiTrack and using frontal angular velocity, as shown in Fig. 4(e) and (f). Most of the differences lie between -1 and 1 samples (the sampling rate is 60 Hz). Henceforth, the instants of peaks and valleys can be used as estimates of MinDI and MaxDI.

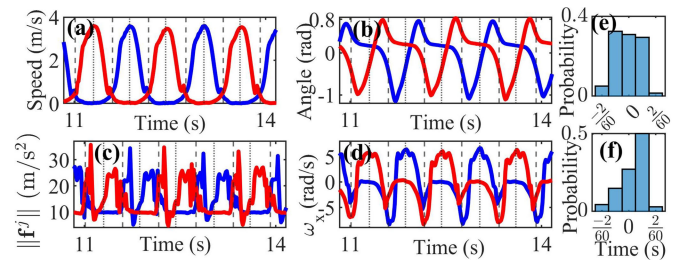


Fig. 4. Changes in (a) horizontal speed, (b) pitch angle, (c) norm of specific force, and (d) frontal angular speed of the feet during walking. The blue, red, dashed, and dotted lines represent the right foot, left foot, MaxDI, and MinDI, respectively. Therein, the frontal angular velocity is suitable for detecting MaxDI and MinDI, and (e) and (f) gaps between corresponding detection and the truth are shown in blue histogram.

TABLE I
QUALITY COMPARISON OF DISTANCE CURVES FIT
BY DIFFERENT MODELS

	Polynomial	Fourier	Gaussian	Σ Sine
Number of coefficients	7	6	6	9
R ²	0.9995	0.9997	0.9996	0.9998
RMSE	0.0037	0.0031	0.0035	0.0025

B. Construction of the Time-Varying Bound

In this section, we propose a varying distance curve model where the central idea is to model a standard pattern within one stride and then deform it according to certain rules to adapt it to different situations. The pattern and the adaptive deformation rules will be explained in this section, and more evaluation of the pattern will be shown in Section V.

According to the traditional and natural strides division as described in Section II-A, one stride is between two consecutive MaxDIs. We modeled the change in this division in our previous work [24]. However, the maximum distances show greater fluctuations compared to the minimum distances, as shown in Fig. 5(a) and paper [37]. This brings problems for modeling and adaptive deformation. Therefore in this article, we choose to model a standard pattern between two consecutive MinDIs, which is modeled as $\gamma_n = f_n(u) + w_\gamma$, where w_γ is a zero-mean Gaussian random variable with variance σ_γ^2 , u is an auxiliary variable for constructing the distance curve which is limited to $\{u | 0 \leq u \leq \pi, u \in \mathbb{R}\}$ for ease of fitting, and $f_n(u)$ is the standard curve.

We used straight walking data from OptiTrack system to fit the curve. The data were split at MinDIs, and were all standardized to $[0, \pi]$ as shown in gray dot lines in Fig. 5(a). We compared fitting the average curve (green solid line) using polynomial, Fourier, Gaussian, and the sum of sines models, and the qualities of the fits are shown in Table I. Among these four types of models, Fourier and the sum of sines models have higher R² and smaller RMSE, of which the Fourier model requires fewer coefficients. Therefore, we chose the Fourier model to generate the pattern. Next, the curve is normalized to $[0, 1]$ in the y-axis direction. The fit distance curve is

$$\begin{aligned}
 f_n(u) = & 0.1219 \sin(1.862u) - 0.4935 \cos(1.862u) \\
 & - 0.08383 \cos(3.724u) + 0.04255 \sin(3.724u) \\
 & + 0.5857.
 \end{aligned} \tag{20}$$

Note that using the proposed in-stride curve in an estimator introduces one step (half-stride) delay to the estimator in space as it needs to wait for the arrival of the next MinDI before continuing the run. As a step is only a few tens of centimeters, the delay does not affect the real-time nature of pedestrian positioning. However, the IMU data received in the current step should be temporarily stored until a new MinDI is detected, and only then the navigation state estimation starts. Taking the rear step of a certain left stride as the current step as an example, Fig. 1 illustrates the time-evolving trajectories and distance curve γ_k using a color bar from orange to green to encode time. At each instants, the positions of the trajectories and the distance between two feet are marked with a corresponding color from the color bar.

The standard pattern can be adaptively deformed to each stride according to the detected MaxDI and MinDI described in Section IV-A by an affine transformation

$$\begin{bmatrix} u_d^* \\ \gamma_d^* \\ 1 \end{bmatrix} = \begin{bmatrix} a_{11} & a_{12} & a_{13} \\ a_{21} & a_{22} & a_{23} \\ 0 & 0 & 1 \end{bmatrix} \begin{bmatrix} u_n^* \\ \gamma_n^* \\ 1 \end{bmatrix} \quad (21)$$

where (u_n^*, γ_n^*) is a discrete point uniformly sampled from the standard pattern at a custom frequency (higher than that of IMU, e.g., $2/T_s$), and (u_d^*, γ_d^*) is the point after deformation. The elements of the affine matrix a_{ii} can be computed from known three pairs of points. The three points can be the vertices of the triangles as shown in Fig. 5(b), which are the points at the maxima and with horizontal coordinates 0 and π , respectively. The deformation is for discrete points and the discrete auxiliary variables (horizontal coordinates) are no longer uniformly distributed after the deformation. We need a new uniformly distributed auxiliary variable u_s^* for interpolating (e.g., linearly) samples in the data points after deformation to generate distance measurements at the same frequency as the IMU. That is, assuming that one stride contains S IMU samples, then we need to sample S points on the deformed curve uniformly between 0 and π . These auxiliary variables are illustrated in Fig. 5(c) and the respective values are shown in Fig. 5(b). We call this *full deformation*.

The variation of MaxDIs in strides can be neglected since they are at the ends of the stance phase of two feet and the amplitude variation is very small. In this *simple deformation*, (21) is simplified to a scale change in the y -axis direction

$$\begin{bmatrix} u_s^* \\ \gamma_k \\ 1 \end{bmatrix} = \begin{bmatrix} 1 & 0 & 0 \\ 0 & \gamma_{\max} - \gamma_{\min} & \gamma_{\min} \\ 0 & 0 & 1 \end{bmatrix} \begin{bmatrix} u_n^* \\ \gamma_n^* \\ 1 \end{bmatrix}. \quad (22)$$

The setting of γ_{\min} and γ_{\max} is flexible. As mentioned in work [23], the standard deviations (1σ) of γ_{\min} between feet are less than 15 mm for one person and they set this bound to be the mean of the first three gait cycles after the user begins to walk. However, the initial positions of the feet are set artificially and the estimated coordinates of the first three cycles are drifting because they are not constrained, and hence the calculated minimum distances also gradually diverge although not significantly. The γ_{\max} is actually the step length which itself is hard to estimate. Many linear and nonlinear formulations as well as machine learning methods [3] have

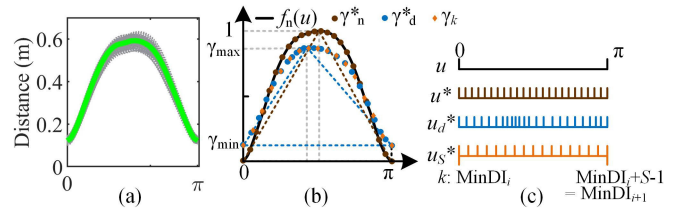


Fig. 5. (a) All one-stride distance curves (gray) between two insteps are normalized in the same interval, and their mean value is displayed in green. (b) Fit standard distance curve, the auxiliary points, and (c) auxiliary variables arising from the deformation process employed to obtain the final distance measurements are illustrated. (u_n^*, γ_n^*) is deformed to (u_d^*, γ_d^*) . Then, the final desired (u_s^*, γ_k) is interpolated based on the IMU sampling time.

been proposed for this purpose, but most of them still involve individual parameters or training. Furthermore, these algorithms heavily depend on the sensor position. A foot-specific method can be used to compute adaptive per-step γ_{\max} , but we will empirically set it to a constant in our experiments. For example, the γ_{\min} and γ_{\max} of a user can be roughly estimated by asking the user to arbitrarily walk straight ahead for a few steps at a constant pace during idle time. The results in Section V show that our method still outperforms other methods with this simple setting.

Although our simulated pseudo-measurements are not as accurate as the real-time true measurements in papers [19], [20], [21], [22], our method can constrain the divergence of the trajectories at each instant without additional sensors, making it more temporally accurate than using MaxDC and MinDC.

V. EXPERIMENTAL RESULTS

In this section, we describe our experimental datasets and also report the results of comparing the proposed methods to alternative methods.

A. Experimental Setup and Evaluation Overview

To evaluate the methods, we compared the results of the MaxDC [15] method, the minimum constraint (MinDC) [37] method, and our SVDC. We used two Xsens DOT sensors to collect the movement data. The two IMUs were placed as shown in Fig. 1. The data were sampled at 60 Hz and sent to a mobile phone via Bluetooth. We evaluated the methods with 2-D (horizontal) errors in different cases: Subject1 walking along a 4.5×6 m rectangle with normal pace, along an S-shaped path containing many 180° turns, and along a random path involving abnormal steps, and running along the rectangle, which are with reference positions of the IMUs captured by the OptiTrack system; Subject2 walking along a 400 m running track; and setting the methods with different parameters. The details are explained in Sections V-C–V-G. All datasets are publicly available.²

B. IMU Calibration and Initial Alignment

We calibrated the sensor biases before collection. For gyroscopes, we used a static period before the movement to calculate the biases. For accelerometers, we collected long

²<https://github.com/xf-ma/DualFeetIMUDataset>

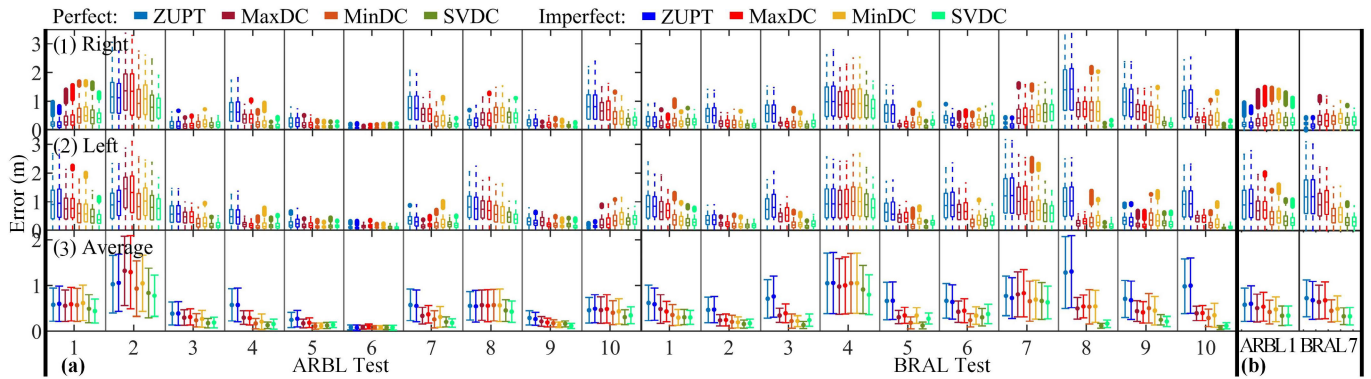


Fig. 6. Statistical errors for each test in the datasets of walking along the rectangular path when (a) IMU A is placed on the right foot and IMU B is on the left foot (ARBL) and when the IMUs are swapped (BRAL), and (b) two selected tests when the right foot is informed to have a higher confidence level. Row (1) shows box plots of each set of tests for the right foot and row (2) shows them for the left foot. Row (3) shows the average error bars, where the mean and variance are the averages of the two feet. In the legend, “perfect” means that the distance curves, distance extrema instants, and zero-velocity intervals are reconstructed using true data (from OptiTrack system), and “imperfect” means that they are estimated using the proposed method.

static data in random orientations and calculated biases using nonlinear least squares through $g = \|f_k^j - b_a^j\|$, where g is local gravitational acceleration, and f_k^j and b_a^j are the vectors of the outputs and the biases of j th accelerometer, respectively.

A wrong initial heading leads to a rigid rotation of the whole trajectory. This may lead to heading and position errors that outweigh the drift caused by the gyroscope errors. The alignment of the initial heading angle is ignored (just set it as 0) or not explicitly stated in some studies of 6DoF-IMU-based positioning methods. To focus on the position error caused by IMU errors such as the deflection caused by z -axis gyroscope bias, the setting of the initial heading should be done carefully. Here, we use a similar method as in paper [37] and [40], where the first stride is used for determining the initial heading.

C. Experiment 1: Walking Along a Rectangular Path

In this section, we evaluate the point-to-point errors of walking along a rectangular path. The ground truth is provided by the OptiTrack system. We took 20 sets of measurements and the subject walked around the rectangle 20 laps for about 400 m in each measurement. To avoid the effect of residual bias error of the IMUs, between the experiments, we exchanged the sensors on the feet, that is, placed IMU A on the right foot and IMU B on the left foot (ARBL) for Test 1–10, and placed IMU B on the right foot and IMU A on the left foot (BRAL) for Test 11–20.

Since the performance of the methods is influenced by several factors, such as the detection of GE, ZVI, and distance curve model error, we evaluated the methods using both perfect and imperfect detections. The perfect detection means constructing the ZVI, MinDI, and foot-to-foot distance curve from OptiTrack data directly. The purpose is to compare the effects of the constraint methods per se. The imperfect detection means detecting ZVI and GE via Section IV-A and constructing a distance curve via Section IV-B, which might be inaccurate but more realistic. Besides, we use fixed γ_{\max} , fixed γ_{\min} , and simple deformation to generate the distance curves.

Fig. 6(a) shows the point-to-point statistical error for each measurement with ARBL and BRAL placements. Each

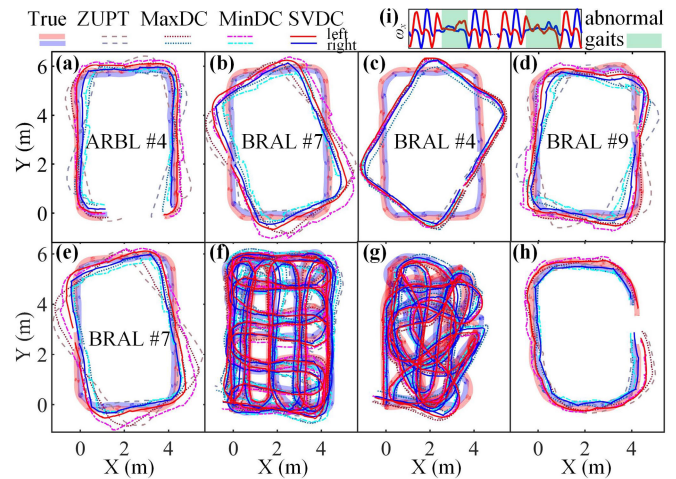


Fig. 7. Part of the estimated trajectories when (a) feet drift equally to different sides, (b) feet drift to one side to different degrees, (c) feet drift equally to one side, (d) feet drift to two sides to different degrees, (e) right foot is informed to have a higher confidence level, (f) walking along an S-shaped path, (g) walking along a random path contains abnormal gaits shown in (i), and (h) running along the rectangular path. The distance curves, distance extrema instants, and zero-velocity intervals are estimated using the proposed methods. Our method is more capable than the other methods in correcting both feet’s trajectories to be closer to the truth.

column is for one test. The first row shows the box plot of the right foot in each test, and the second row shows that of the left foot. Due to the zero-bias instability, random walk of the gyroscope, or other random factors, several different cases may occur where the trajectories: 1) drift equally to different sides; 2) drift to one side to different degrees; 3) drift equally to one side; and 4) or drift to different sides to different degrees. For case 2), the trajectory of one foot estimated by ZUPT must be closer to the truth compared to the other foot. For example, the ZUPT result is the best and the constraint methods are worse for the right foot in BRAL Test 7 in Fig. 6(a), while the situation is the reverse for the left foot. We therefore also show the average error bar in the third row, where the mean and standard deviation are the averages of the two feet.

From Fig. 6(a), we see that Test 6 of ARBL shows the smallest and almost the same errors for all methods. This is because the drift of both feet in this test happens to be

TABLE II
OVERALL STATISTICAL ERROR ACROSS ALL TESTS

	perfect ARBL			perfect BRAL			imperfect ARBL			imperfect BRAL		
	mean	max	std	mean	max	std	mean	max	std	mean	max	std
ZUPT _L	0.483	1.266	0.287	0.803	2.033	0.484	0.496	1.311	0.299	0.818	2.039	0.485
ZUPT _R	0.469	1.307	0.293	0.703	1.777	0.424	0.468	1.294	0.304	0.683	1.785	0.428
ZUPT _A	0.476	1.286	0.290	0.753	1.905	0.454	0.482	1.302	0.302	0.751	1.912	0.457
MaxDC _L	0.450	1.082	0.249	0.528	1.263	0.285	0.444	1.119	0.249	0.552	1.276	0.294
MaxDC _R	0.411	1.080	0.245	0.407	1.009	0.229	0.429	1.183	0.271	0.408	1.020	0.237
MaxDC _A	0.430	1.081	0.247	0.467	1.136	0.257	0.437	1.151	0.260	0.480	1.148	0.266
MinDC _L	0.348	1.012	0.215	0.390	1.247	0.256	0.378	1.095	0.236	0.420	1.241	0.259
MinDC _R	0.352	1.038	0.225	0.417	1.266	0.276	0.379	1.072	0.236	0.433	1.253	0.274
MinDC _A	0.350	1.025	0.220	0.403	1.256	0.266	0.378	1.084	0.236	0.427	1.247	0.266
SVDC _L	0.338	0.911	0.206	0.322	0.876	0.196	0.344	0.947	0.209	0.361	0.914	0.202
SVDC _R	0.319	0.898	0.200	0.314	0.833	0.188	0.331	0.911	0.204	0.348	0.846	0.194
SVDC _A	0.328	0.905	0.203	0.318	0.854	0.192	0.337	0.929	0.207	0.355	0.880	0.198

Note: The A in the subscript denotes average, the R is right foot, and the L is left foot. ARBL means that IMU A is placed on the right foot and B is on the left foot, and BRAL is vice versa. The distance curves, distance extrema instants, and zero-velocity intervals are constructed from the OptiTrack system (perfect) or the proposed methods (imperfect). All the units are meters.

extremely small, and the ZUPT estimate is already pretty close to the truth. However, this is a rare and serendipitous occurrence that happened by chance. Among other tests, the average error of our method is lowest or comparable to other constrained methods in most tests regardless of whether we use perfect or imperfect detection. Additionally, imperfect detection indeed results in slightly worse performance, both in terms of separate foot errors and averaged errors. However, the resulting difference is small and it does not change the performance ranking of the four methods in each test.

Table II further shows the statistical error over all the tests, where the mean, max, and std of each method are averaged over ten tests of the corresponding indicator. The ranking of the three constraint effects is MaxDC < MinDC < SVDC. MaxDC and MinDC apply constraints only when the estimated distance between the feet exceeds the preset bound. Among them, the MinDC method can restrain the divergence of the position more timely than the MaxDC method, whereas our method acts as a constraint at every moment. Therefore, our method demonstrates better results under all the three metrics.

For clearer presentation, only a subset of the calculated trajectories (with imperfect detection) are displayed in Fig. 7(a)–(d), and they are around the 20th laps which have more drift accumulated compared to the trajectories at the start. The four subplots in Fig. 7(a)–(d) show the four different combinations of drifting of the two feet mentioned earlier. Fig. 7(c) is the subset of the trajectories corresponding to Test 4 of BRAL placement, and we can see that none of the three constraints works significantly better for the case of drifting in the same degree to the same direction. In other cases, our method estimates bipedal trajectories that consistently maintain a spacing close to the physical reality, with divergence suppressed more timely, resulting in smoother trajectories.

D. Case Study: If the Feet Are Weighted

In Section III-D, we discussed a scenario where the confidence of the feet can be estimated by some strategy. Although developing this strategy is a topic of future research, we now

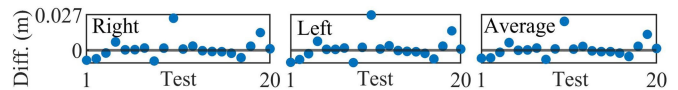


Fig. 8. Difference for each test of using the proposed fully and simply deformed distance curves. They have almost the same outcome. (Test 1–10: IMU A on right B on left, Test 11–20: IMU B on right A on left.)

show the results with artificially set confidence weights to compare the performance of the three constraints in this case.

We simulate the situation where the right foot has higher confidence. We selected some tests in which both feet drift to different degrees and the ZUPT of the right foot is closer to the truth. Then, we artificially reduced the variance of the right gyroscope by 0.3 and amplified it on the left foot by 1.7. This is equivalent to the right foot having a higher confidence, and the constraint will produce smaller corrections to the right foot and larger corrections to the left foot. Intuitively, the constrained trajectories should be pulled together toward the right foot trajectory rather than to the middle of the two.

Fig. 6(b) shows the errors of the four methods under this confidence setting. Together with Fig. 6(a), we can see that the performance of our method is further improved when the proposed confidence is added. Fig. 7(e) shows the estimated trajectories of different methods in Test 7 of BRAL set, and Fig. 7(b) shows the estimated trajectories with equal confidence for both feet of this test. Our method more effectively constrains the trajectory to the relatively better one. Since MinDC only implements constraints at certain moments, the “pull” effect on the trajectory is not continuous. Our method continuously pulls the trajectory in a direction with higher confidence, thus showing better results.

E. Comparison of Fully and Simply Deformed Distance Curve

In this section, we compare the effect on trajectory estimation of using the constructed distance curves with the full and simple deformations described in Section IV-B.

Fig. 8 shows the difference between the mean errors of these two methods on each test. It can be seen that the maximum difference is within 0.025 m. The full deformation requires more computational resources but does not result in a more significant improvement, so we can conclude that the simple deformation is sufficient to produce good constraints.

F. Experiment 2: Different Subject

In this section, we show the results of another subject walking along a standard 400 m running track counterclockwise five times and clockwise five times. Due to the unavailability of ground truth, we do not give quantitative error results, but only show the distribution of trajectories and end points in Fig. 9.

The results show our method can constrain the trajectory effectively. Our estimated trajectories are closer to the real situation in multiple sets of tests from Fig. 9(a). The ending points of our method are more concentrated and close to the truth from Fig. 9(b). Both the first subject in experiment 1 and the second subject here experimented with a normal pace (no sprinting or slow walking). It can be seen from the results that

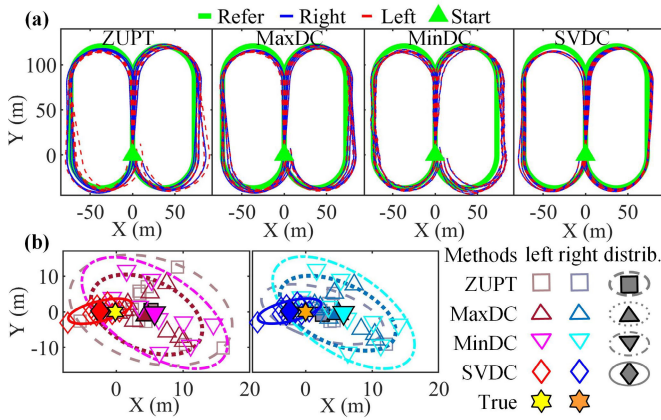


Fig. 9. (a) Trajectories and (b) ending points of subject 2 walking along a standard 400 m running track. All ten tests are shown together. Our approach yields more compact estimates on multiple sets of tests than the other methods.

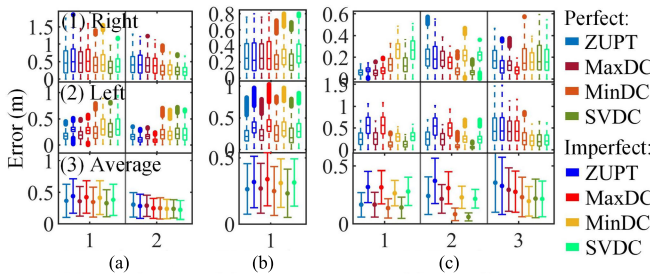


Fig. 10. Statistical errors for tests of (a) S-shaped path, (b) random path contains hesitations, sudden retreats, and sideways slips, and (c) running along the rectangular path. For the legend, see the caption of Fig. 6.

the distance curve model proposed in Section IV-B can adapt to different people when the IMUs are placed on the insteps and the person walks at a normal speed.

G. Experiment 3: Challenging Cases

It is reasonable to suspect that our model may introduce errors in other situations since our model is only fit using data from a healthy individual walking straightforward at a constant speed. We therefore conducted the following challenging tests to evaluate our methods for more conditions and speeds: 1) walking along an S-shaped path containing many 180° turns; 2) walking randomly which contains abnormal steps such as hesitations, sudden retreats, and sideways slips; and 3) running tests along the rectangular path. Fig. 7(f)–(h) shows the estimated trajectories of some tests of these paths.

These scenarios are not ideal cases for our methods. At corners, the minimum and maximum distance in one stride and the occurrence instants change more noticeably than going straight, which affects the height of the distance curve. Speed changes mainly lead to the distance curve having a more pointy (thin) shape. In these cases, the pseudo-measurements provided by our distance model are less credible. A simple way to cope with this is to adaptively increase the variance of the model. A more advanced way would be to use online data to adjust the distance curve adaptively, but we will leave that to future work. Here, we only use our current model to see its performance in these challenging scenarios. Furthermore, the

gait pattern changes in abnormal steps (compare Fig. 7(i) and Fig. 2), creating difficulties for our distance extrema instants detection method. One approach is to detect abnormal gaits by a classifier and disable the constraint part in these steps. Here, we manually labeled the abnormal steps.

From Fig. 10, we can see that our methods perform far from perfect detection in some tests because they face the challenge of misdetection and misconfiguration of the distance curve in these scenarios. However, the results show that our method still works well and maintains relatively better performance than the other methods with both perfect and imperfect detection.

VI. CONCLUSION

In this article, we proposed a dual-feet-based positioning method with SVDC. The proposed SVC can ensure that the feet are physically confined to the left and right at MinDIs. The proposed time-varying distance curve offers pseudo-distance measurement at each instant. The proposed method was compared with other similar methods (MaxDC and MinDC). Our method is better at constraining the spacing between the feet. We also developed a method that can take the relative confidence of the feet trajectories into account and therefore correct the feet trajectories better toward the true trajectory.

Our approach shows good performance in controlling foot spacing without additional sensors, which is achieved mainly by correcting the positions of the feet. However, its actual effect on the heading drift remains to be proven by observability analyses. Furthermore, the height and pointiness of the distance curve deform in more complex scenarios such as turning or speed changes. The pseudo-measurements generated will contain a high level of noise if the distance curve model is not adjusted accordingly. We will address these issues in our future work. For example, we can adjust the variance of the distance model according to different scenarios, which requires an activity classifier, or build more adaptive and accurate distance models, for example, via physics-informed machine learning or Gaussian process regression taking the kinematics of the distance between the feet into account.

REFERENCES

- [1] P. D. Groves, *Principles of GNSS, Inertial, and Multisensor Integrated Navigation Systems* (GNSS Technology and Application Series), 2nd ed., Boston, MA, USA: Artech House, 2013.
- [2] N. Samama, *Indoor Positioning: Technologies and Performance*. Hoboken, NJ, USA: Wiley, 2019.
- [3] X. Hou and J. Bergmann, "Pedestrian dead reckoning with wearable sensors: A systematic review," *IEEE Sensors J.*, vol. 21, no. 1, pp. 143–152, Jan. 2021.
- [4] A. Correa, M. Barcelo, A. Morell, and J. Vicario, "A review of pedestrian indoor positioning systems for mass market applications," *Sensors*, vol. 17, no. 8, p. 1927, Aug. 2017, doi: [10.3390/s17081927](https://doi.org/10.3390/s17081927).
- [5] J. Wahlström and I. Skog, "Fifteen years of progress at zero velocity: A review," *IEEE Sensors J.*, vol. 21, no. 2, pp. 1139–1151, Jan. 2021.
- [6] M. Xia, C. Xiu, D. Yang, and L. Wang, "Performance enhancement of pedestrian navigation systems based on low-cost foot-mounted MEMS-IMU/ultrasonic sensor," *Sensors*, vol. 19, no. 2, p. 364, Jan. 2019. [Online]. Available: <https://europepmc.org/articles/PMC6359363>
- [7] N. Akai and K. Ozaki, "Gaussian processes for magnetic map-based localization in large-scale indoor environments," in *Proc. IEEE/RSJ Int. Conf. Intell. Robots Syst. (IROS)*, Hamburg, Germany, Sep. 2015, pp. 4459–4464.

- [8] A. Solin, M. Kok, N. Wahlström, T. B. Schön, and S. Särkkä, "Modeling and interpolation of the ambient magnetic field by Gaussian processes," *IEEE Trans. Robot.*, vol. 34, no. 4, pp. 1112–1127, Aug. 2018.
- [9] F. Viset, R. Helmons, and M. Kok, "An extended Kalman filter for magnetic field SLAM using Gaussian process regression," *Sensors*, vol. 22, no. 8, p. 2833, Apr. 2022.
- [10] H. Ju, J. H. Lee, and C. G. Park, "Pedestrian dead reckoning system using dual IMU to consider heel strike impact," in *Proc. 18th Int. Conf. Control, Autom. Syst. (ICCAS)*, Oct. 2018, pp. 1307–1309.
- [11] Z. Li, X. Xu, M. Ji, J. Wang, and J. Wang, "Pedestrian positioning based on dual inertial sensors and foot geometric constraints," *IEEE Trans. Ind. Electron.*, vol. 69, no. 6, pp. 6401–6409, Jun. 2022.
- [12] Z. Li, X. Xu, J. Wang, and C. Zhang, "Prior kinematic information fusion for pedestrian localization with Toe-Heel-Shank MIMUs," *IEEE Trans. Ind. Electron.*, vol. 70, no. 7, pp. 7498–7506, Jul. 2023.
- [13] J. Wang, J. Liu, X. Xu, Z. Yu, and Z. Li, "A yaw correction method for pedestrian positioning using two low-cost MIMUs," *Measurement*, vol. 217, Aug. 2023, Art. no. 112992.
- [14] I. Skog, J.-O. Nilsson, D. Zachariah, and P. Händel, "Fusing the information from two navigation systems using an upper bound on their maximum spatial separation," in *Proc. Int. Conf. Indoor Positioning Indoor Navigation (IPIN)*, Sydney, NSW, Australia, Nov. 2012, pp. 1–5.
- [15] G. V. Prateek, R. Girisha, K. V. S. Hari, and P. Händel, "Data fusion of dual foot-mounted INS to reduce the systematic heading drift," in *Proc. 4th Int. Conf. Intell. Syst., Modeling Simulation*, Jan. 2013, pp. 208–213.
- [16] Y. Bolotin, A. Bragin, and D. Gulevskiy, "On consistency of EKF for pedestrian dead reckoning with foot mounted IMU," in *Proc. 27th Int. Conf. Integr. Navigat. Syst. (ICINS)*, Saint Petersburg, Russia, May 2020, pp. 1–10.
- [17] W. Shi, Y. Wang, and Y. Wu, "Dual MIMU pedestrian navigation by inequality constraint Kalman filtering," *Sensors*, vol. 17, no. 2, p. 427, 2017.
- [18] Q. Wang, M. Cheng, A. Noureldin, and Z. Guo, "Research on the improved method for dual foot-mounted inertial/magnetometer pedestrian positioning based on adaptive inequality constraints Kalman filter algorithm," *Measurement*, vol. 135, pp. 189–198, Mar. 2019.
- [19] C.-S. Jao, Y. Wang, and A. M. Shkel, "Pedestrian inertial navigation system augmented by vision-based foot-to-foot relative position measurements," in *Proc. IEEE/ION Position Location Navigat. Symp. (PLANS)*, Portland, OR, USA, Apr. 2020, pp. 900–907.
- [20] M. Zhu, Y. Wu, and S. Luo, "F²IMU-R: Pedestrian navigation by low-cost foot-mounted dual IMUs and interfoot ranging," *IEEE Trans. Control Syst. Technol.*, vol. 30, no. 1, pp. 247–260, Jan. 2022.
- [21] L. Qi et al., "A robust foot-mounted positioning system based on dual IMU data and ultrasonic ranging," *IEEE Sensors J.*, vol. 23, no. 4, pp. 4085–4095, Feb. 2023.
- [22] C. Chen, C.-S. Jao, A. M. Shkel, and S. S. Kia, "UWB sensor placement for foot-to-foot ranging in dual-foot-mounted ZUPT-aided INS," *IEEE Sens. Lett.*, vol. 6, no. 2, pp. 1–4, Feb. 2022.
- [23] X. Niu, Y. Li, J. Kuang, and P. Zhang, "Data fusion of dual foot-mounted IMU for pedestrian navigation," *IEEE Sensors J.*, vol. 19, no. 12, pp. 4577–4584, Jun. 2019.
- [24] X. Ma and S. Särkkä, "Indoor positioning methods based on dual feet-mounted IMUs with distance constraints," in *Proc. 13th Int. Conf. Indoor Positioning Indoor Navigat. (IPIN)*, Sep. 2023, pp. 1–6.
- [25] L. Xing, X. Tu, and Z. Chen, "Foot-mounted pedestrian navigation method by comparing ADR and modified ZUPT based on MEMS IMU array," *Sensors*, vol. 20, no. 13, p. 3787, Jul. 2020.
- [26] L. Wang, H. Tang, T. Zhang, Q. Chen, J. Shi, and X. Niu, "Improving the navigation performance of the MEMS IMU array by precise calibration," *IEEE Sensors J.*, vol. 21, no. 22, pp. 26050–26058, Nov. 2021.
- [27] A. Kharb, V. Saini, Y. K. Jain, and S. Dhiman, "A review of gait cycle and its parameters," *Int. J. Comput. Eng. Manag.*, vol. 13, no. 1, pp. 78–83, 2011.
- [28] N. Mani, P. Haridoss, and B. George, "A wearable ultrasonic-based ankle angle and toe clearance sensing system for gait analysis," *IEEE Sensors J.*, vol. 21, no. 6, pp. 8593–8603, Mar. 2021.
- [29] J. C. Pérez-Ibarra, A. A. G. Siqueira, and H. I. Krebs, "Real-time identification of gait events in impaired subjects using a single-IMU foot-mounted device," *IEEE Sensors J.*, vol. 20, no. 5, pp. 2616–2624, Mar. 2020, doi: [10.1109/JSEN.2019.2951923](https://doi.org/10.1109/JSEN.2019.2951923).
- [30] V. Madyastha, V. Ravindra, S. Mallikarjunan, and A. Goyal, "Extended Kalman filter vs. Error state Kalman filter for aircraft attitude estimation," in *Proc. AIAA Guid., Navigat., Control Conf.*, Aug. 2011, p. 6615.
- [31] M. Kok, F. Viset, and M. Osman, "A framework for indoor localization using the magnetic field," in *Proc. 23rd IEEE Int. Conf. Mobile Data Manage. (MDM)*, Paphos, Cyprus, Jun. 2022, pp. 385–387.
- [32] J.-O. Nilsson, I. Skog, and P. Handel, "A note on the limitations of ZUPTs and the implications on sensor error modeling," in *Proc. Int. Conf. Indoor Position. Indoor Navig.*, Nov. 2012, p. 4.
- [33] A. Jiménez, F. Seco, J. Prieto, and J. Guevara, "Indoor pedestrian navigation using an INS/EKF framework for yaw drift reduction and a foot-mounted IMU," in *Proc. 7th Workshop Positioning, Navigat. Commun.*, Dresden, Germany, Mar. 2010, pp. 135–143.
- [34] D. Simon, *Optimal State Estimation: Kalman, H_∞, and Nonlinear Approaches*, 1st ed., Hoboken, NJ, USA: Wiley, May 2006.
- [35] E. Foxlin, "Pedestrian tracking with shoe-mounted inertial sensors," *IEEE Comput. Graph. Appl.*, vol. 25, no. 6, pp. 38–46, Nov. 2005.
- [36] R. Girisha, G. V. Prateek, K. V. S. Hari, and P. Händel, "Fusing the navigation information of dual foot-mounted zero-velocity-update-aided inertial navigation systems," in *Proc. Int. Conf. Signal Process. Commun. (SPCOM)*, Bangalore, India, Jul. 2014, pp. 1–6.
- [37] T. Liu, J. Kuang, Y. Li, and X. Niu, "A novel minimum distance constraint method enhanced dual-foot-mounted inertial navigation system for pedestrian positioning," *IEEE Internet Things J.*, vol. 10, no. 19, pp. 16931–16944, Oct. 2023.
- [38] D. Simon, "Kalman filtering with state constraints: A survey of linear and nonlinear algorithms," *IET Control Theory Appl.*, vol. 4, no. 8, pp. 1303–1318, Aug. 2010.
- [39] S. J. Julier and J. J. LaViola, "On Kalman filtering with nonlinear equality constraints," *IEEE Trans. Signal Process.*, vol. 55, no. 6, pp. 2774–2784, Jun. 2007.
- [40] W. Li, Z. Xiong, Y. Ding, Z. Cao, and Z. Wang, "Lower limb model based inertial indoor pedestrian navigation system for walking and running," *IEEE Access*, vol. 9, pp. 42059–42070, 2021.
- [41] I. Skog, P. Handel, J. O. Nilsson, and J. Rantakokko, "Zero-velocity detection—An algorithm evaluation," *IEEE Trans. Biomed. Eng.*, vol. 57, no. 11, pp. 2657–2666, Nov. 2010.
- [42] X. Niu, T. Liu, J. Kuang, Q. Zhang, and C. Guo, "Pedestrian trajectory estimation based on foot-mounted inertial navigation system for multi-story buildings in postprocessing mode," *IEEE Internet Things J.*, vol. 9, no. 9, pp. 6879–6892, May 2022.



Xiaofeng Ma (Graduate Student Member, IEEE) received the bachelor's degree from China University of Petroleum, Qingdao, China, in 2018, and the master's degree from Beihang University, Beijing, China, in 2021. She is currently pursuing the Ph.D. degree with Aalto University, Espoo, Finland.

Her current research interests include pedestrian navigation, data fusion, Gaussian process, Bayesian filtering, and computer vision.



Simo Särkkä (Senior Member, IEEE) received the M.Sc.(Tech.) degree (Hons.) in engineering physics and mathematics, and the D.Sc.(Tech.) degree (Hons.) in electrical and communications engineering from Helsinki University of Technology, Espoo, Finland, in 2000 and 2006, respectively.

Currently, he is a Professor with Aalto University, Espoo; and an Adjunct Professor at Tampere University of Technology, Tampere, Finland; and Lappeenranta University of Technology, Lappeenranta, Finland. He has authored or co-authored over

150 peer-reviewed scientific articles and his books *Bayesian Filtering and Smoothing* and *Applied Stochastic Differential Equations* have been published via the Cambridge University Press. His research interests are in multisensor data processing systems with applications in location sensing, health and medical technology, machine learning, inverse problems, and brain imaging.